Master Thesis

Ewout van den Pol

Estimating Lower-body Kinematics During Walking Using a Small Set of IMUs

Engineering Technology – Biomechanical Engineering

dr. E.H.F. van Asseldonk
prof.dr.ir. P.H. Veltink
J. Zhang MEng

April 14, 2025

UNIVERSITY
OF TWENTE.

Contents

1 Introduction

Gait analysis is a valuable tool for researchers. It has been applied in different fields, such as robotics and healthcare [1], [2], [3]. To conduct gait analysis effectively, the kinematics during walking should be captured, especially the lower-body kinematics. The industry standard for human motion capture in the laboratory is optical motion capture (OMC) systems [4]. Another viable option is using inertial motion capture (IMC) systems, which are based on Inertial Measurement Units (IMUs) [5]. Using OMC or IMC systems enables researchers to derive lower-body kinematics, such as orientation, acceleration, angular velocity and position of each segment [6].

Most OMC systems use markers applied to the subject to capture the pose of the subject and derive the kinematic data. Although accurate, OMC systems have some limitations. A limitation is the need for trained personnel to apply the markers in the correct placement. This marker placement should be perfect for obtaining accurate results during pose reconstruction [7]. This results in an expensive and time-consuming system. In addition, the OMC system has a limited range and needs a clear line of sight to work correctly.

Alternatively, the IMC systems offer advantages compared to the OMC systems, such as being easier to configure, cheaper [8], and not having a range limit in which the movement of the person can be assessed. IMUs can measure linear acceleration, angular velocity, and heading based on the magnetic field [9], which are measured using an accelerometer, gyroscope, and magnetometer, respectively. This is potentially advantageous as they are directly related to segmental kinematics when estimating the segmental velocities, positions and angular velocities. However, a drawback of using IMUs is that strapdown inertial navigation will result in drift in the parameters obtained from the IMUs. This is caused by the integration of the acceleration. Because the acceleration signal also contains sensor noise and bias, direct integration of this signal will result in drift in the estimated velocity or position [10].

Over time, smaller IMUs became available due to technological advancements [11]. This miniaturization of IMUs looks promising for the use of IMUs for the continuous tracking of daily living tasks [12]. Commercial IMC systems generally use one sensor on each body segment [13]. For instance, for measuring lower-body kinematics, 7 IMUs in total are needed. These are placed at the pelvis, thighs, shanks and feet. Yet, for monitoring daily living tasks, this is too extensive and expensive due to the number of sensors used [11]. The use of fewer IMUs than one sensor per segment could result in a cheaper and more appropriate solution.

There is existing literature using fewer IMUs to estimate lower-body kinematics. For example, using three IMUs, Refai et al. [14] were able to measure relative feet and Centre of Mass (CoM) positions by using the Centroidal Moment Pivot (CMP) point, which relates the movement of the CoM to the stance foot. Combining this information with an Extended Kalman Filter (EKF) enables estimating the positions of the CoM and the feet [15]. But this method does not estimate other lower-body kinematics, such as joint angles or positions of the joints. This is because using only three IMUs results in an underdetermined system when estimating lower-body kinematics because not all lower-body segments are tracked directly.

A method to address the underdetermined system is to make use of distance inequality constraints. Using two foot-mounted IMU-based navigation systems, the system was constrained by using an upper bound for the maximum foot-to-foot distance [16]. Another method is to derive step length based on the inverted pendulum model of human motion [17]. This was made possible by modelling human gait motion as an inverted pendulum and estimating the step length. Based on this estimated step length, a relative position vector between the two feet is used as a constraint. However, these methods are not suitable for continuous tracking and may not accurately reflect actual foot positions [15]. In other research [11], three IMUs were used to track seven segments of the lower extremity. The IMUs were placed on each foot and the pelvis. For sufficient information, constant leg lengths and hinged knee and ankle joints were used, as well as common updates such as zero-velocity and zero-height updates. The positions of the segments were then calculated using the estimated foot and pelvis positions through an inverse kinematics method. However, the Xsens Awinda system with seven IMUs was used for data collection. This means that the efficiency and accuracy of estimating pelvis and foot positions using only three IMUs may not be adequately evaluated and could be redundant, as the Xsens sensor fusion algorithm also uses gait characteristics-based and constraint updates.

This paper aims to estimate the positions of the CoM, hips, knees, ankles, and feet, as well as the joint angles of the hips, knees, and ankles, using a reduced set of IMUs. Additionally, it seeks to determine the orientations of the pelvis, thighs, shanks, and feet. These estimations are based on the accelerations and orientations provided by three IMUs, which are positioned on each foot and one on the back near the pelvis. Firstly, based on the method of Refai et al. [15], the positions of the feet were estimated. Additionally, the method was extended with a pseudo-measurement to estimate the position of the CoM. Furthermore, to estimate the joint angles, a forward kinematics chain-based constrained Kalman filter (FKC-KF) was used. The filter used the hinged knee and ankle constraints combined with a forward kinematics chain-based approach. Finally, the joint positions and segment orientations were estimated using the positions and orientations of both feet and the CoM, along with the estimated joint angles.

This paper uses the online dataset collected by Sy et al. [8]. This allows for a comparison between his methods and our proposed approach, which builds upon the work of Refai et al. [15].

2 Method

2.1 Setup

The data used in this paper were collected by Sy et al. [8]. This experiment consisted of nine healthy subjects (seven male and two female), with an age of 24.6 $\pm$ 3.9 years old, height of 1.70 $\pm$ 0.06 m and weight of 63.0 $\pm$ 6.8 kg. Data was collected by two systems:
1) The Vicon Vantage system, which used eight cameras to cover a 4 by 4 m^2 area. This data was collected at 100 Hz.
2) The Xsens Awinda system, which used seven MTx units (IMUs). This data was also collected at 100 Hz. The accelerations and orientations of each foot and pelvis IMU were used. Also, the step detection for each foot was used. This step detection was manually edited by Luke Sy [8] to remove errors. The Vicon data was used as reference data.

The used movements are: walk straight and back (Walk), walk in figures of eight (Figure of Eight), walk in a zig-zag pattern (Zigzag), and finally an undirected five-minute long walk (FiveMin) with side steps and stand motion. Each trial was performed twice per subject. The seven IMUs were located at the pelvis, thighs, shanks and feet, as can be seen in Figure 3 of [8]. The relevant IMU locations for this research can be seen in Figure 1 and are located on each foot in between the toes and the ankle, and on the middle of the lower back of the subject, which is assumed to be coincident with the mid-pelvis [8].

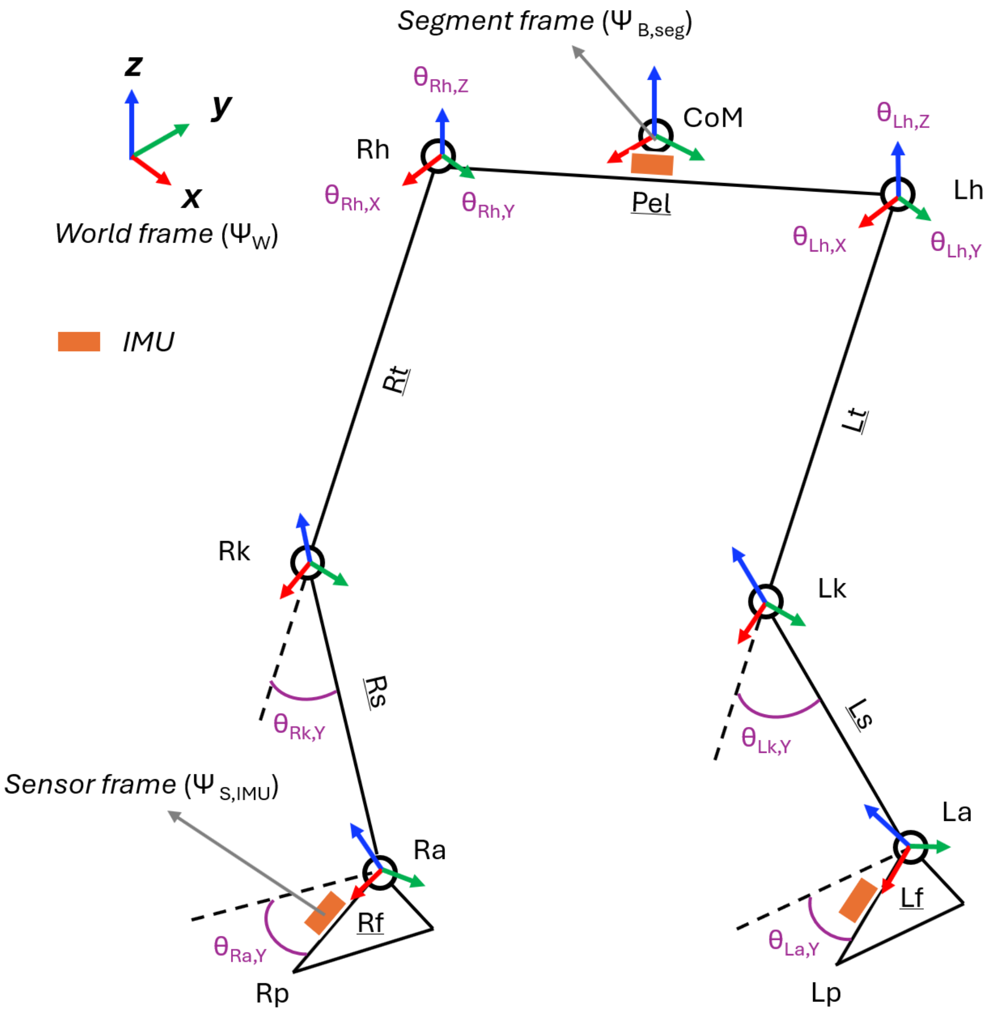

Figure 1: Overview of joints, angles and segments. The joints are represented by circles, and the CoM is also represented as a circle. The segments are represented by a black line between joints and can be recognised by the underlining. The joint angles used in this paper are given in purple. Finally, the locations of the IMUs are given by an orange rectangle.

2.2 Reference frames

There are three reference frames which were used. In Figure 1 we have the world frame (Ψ_W), sensor frames ($\Psi_{S,IMU}$) and the segment frames ($\Psi_{B,seg}$). For the sensor frames, IMU is replaced by Pel, Lf or Rf, representing the pelvis, left foot and right foot, respectively. For the segment frames, seg can be replaced by Pel, Rt, Rs, Rf, Lt, Ls or Lf, representing the pelvis, right thigh, right shank, right foot, left thigh, left shank and left foot, respectively.

The world frame (Ψ_W) was set equal to the Xsens frame [8], which is an East-North-Up (ENU) frame. This means that $+X_W$ pointed to the east, $+Y_W$ pointed to the north, and $+Z_W$ pointed upwards. The sensor frames were aligned corresponding to the Movella Awinda manual [18]. The segment frames were aligned with the anatomical axes of the subject, i.e. $+X_{B,seg}$ pointed forward (anteroposterior), $+Y_{B,seg}$ pointed to the left side of the body (mediolateral), and $+Z_{B,seg}$ pointed upwards (anteroposterior axis).

2.3 Simplified model parameters and notations

In Figure 1, an overview is given of the simplified model. The positions of the CoM, both hips, both knees and both ankles are visualised. Their positions are represented as:

$P = \{{}^W\boldsymbol{p}_{CoM}, {}^W\boldsymbol{p}_{Rh}, {}^W\boldsymbol{p}_{Rk}, {}^W\boldsymbol{p}_{Ra}, {}^W\boldsymbol{p}_{Lh}, {}^W\boldsymbol{p}_{Lk}, {}^W\boldsymbol{p}_{La}\}$

This means, for example, that ${}^W p_{Lk}$ represents the position of the left knee with respect to frame W.

The joints of the simplified model are connected by seven segments: the pelvis, both thighs, both shanks and both feet. The relative distances between the positions P are represented as:

$D = \{\bar{\boldsymbol{d}}_{Rh/CoM}, \bar{\boldsymbol{d}}_{Rk/Rh}, \bar{\boldsymbol{d}}_{Ra/Rk}, \bar{\boldsymbol{d}}_{Lh/CoM}, \bar{\boldsymbol{d}}_{Lk/Lh}, \bar{\boldsymbol{d}}_{La/Lk}\}$

Furthermore, each segment orientation with respect to the world frame in quaternions is represented as:

$SO = \{{}^W\boldsymbol{q}_{Pel}, {}^W\boldsymbol{q}_{Rh}, {}^W\boldsymbol{q}_{Rk}, {}^W\boldsymbol{q}_{Ra}, {}^W\boldsymbol{q}_{Lh}, {}^W\boldsymbol{q}_{Lk}, {}^W\boldsymbol{q}_{La}\}$

The relative distance between the foot IMU locations and the phalanges (toes) and ankles can be calculated, which will be used to estimate their positions from the estimated foot positions. These are represented as:

$I = \{\bar{\boldsymbol{d}}_{IMU/Rp}, \bar{\boldsymbol{d}}_{IMU/Ra}, \bar{\boldsymbol{d}}_{IMU/Lp}, \bar{\boldsymbol{d}}_{IMU/La}\}$

The joint angles for the hip are based on a hip joint with three degrees of freedom (DoF), so around the X-axis (abduction/adduction), Y-axis (flexion/extension) and Z-axis (internal/external rotation). The knee and ankle are represented as hinge joints, so only 1 DoF around the Y-axis. The joint angles for each foot are represented as:

$\Theta_L = \{\theta_{Lh,X}, \theta_{Lh,Y}, \theta_{Lh,Z}, \theta_{Lk,Y}, \theta_{La,Y}\}, \;\; \Theta_R = \{\theta_{Rh,X}, \theta_{Rh,Y}, \theta_{Rh,Z}, \theta_{Rk,Y}, \theta_{Ra,Y}\}$

2.4 Calibration and synchronisation

To synchronise both Xsens and Vicon recordings, a trigger pulse was sent by the Xsens Awinda station to the Vicon system [8]. The Vicon data was used as reference data. The following calibration procedures were performed by Sy et al. [8]. To enable pose comparison between the IMU and Vicon data, a fixed rotational offset was used to convert the Vicon data from the Vicon frame to the world frame. This was based on a calibration procedure using the direction of gravity and the Earth's magnetic field, measured using a compass and a pendulum with optical markers attached [19]. A yaw offset [8], i.e., an offset in rotation around the Z-axis, was used to correct the potential misalignment between body orientation and sensor orientation. A grid search was used to identify the yaw offset that minimized the x and y root mean square error (RMSE) (1) between the Vicon-based acceleration and IMU acceleration. Then, the initial IMU orientation was adjusted using this yaw offset for both feet and pelvis orientations and to minimise pose differences due to calibration.

$$RMSE_{x,y}(\boldsymbol{a}_{Lf,Vicon} - (\boldsymbol{q}_{yaw} \otimes \tilde{\boldsymbol{a}}_{Lf,IMU} \otimes \boldsymbol{q}_{yaw}^{-1}) \tag{1}$$

2.5 Pre-processing

2.5.1 Segment orientation

The frames of the body segment and the attached IMU were misaligned. To solve this misalignment, a sensor-to-segment realignment was used, based on [13]. This was realised for the initial orientation using the Vicon system for a known body segment orientation with respect to the world frame (${}^W\boldsymbol{q}_B$) and the measured sensor orientation with respect to the world frame (${}^W\boldsymbol{q}_S$). Then, the rotation from sensor to segment (${}^B\boldsymbol{q}_S$) can be determined using (2).

$${}^W\boldsymbol{q}_B = {}^W\boldsymbol{q}_S \otimes {}^B\boldsymbol{q}_S^{-1} \tag{2}$$

2.5.2 Step Detection (SD)

The step detection information provided by Sy et al. [8] is used. A step is detected when the variance of the free body acceleration of a foot is below 1 m/s^2 during a 0.25-second window. The false positives/negatives were manually corrected by Luke Sy. These occurred mainly during the five-minute walk.

2.5.3 Gravity-free acceleration

The IMU acceleration signal still contained gravitational acceleration. Therefore, to obtain the body acceleration (${}^{W}\boldsymbol{a}$), the gravitational acceleration was subtracted and afterwards expressed in the world frame, based on [13]. This is shown in (3).

$$ {}^{W}\boldsymbol{a} - {}^{W}\boldsymbol{g} = {}^{W}\boldsymbol{q}_S \otimes ({}^{S}\boldsymbol{a} - {}^{S}\boldsymbol{g}) \otimes {}^{W}\boldsymbol{q}_S^{-1} \tag{3} $$

2.6 Kalman filter

In Figure 2, an overview is given of the algorithm.

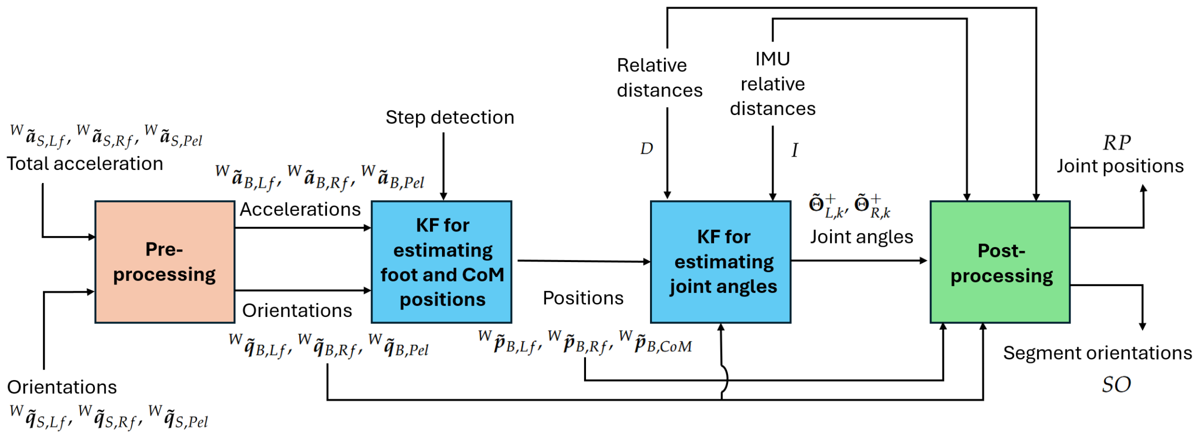

Figure 2: Overview of the algorithm. It starts with the acceleration and orientation information obtained from the IMUs. In pre-processing, the gravity part of the acceleration is removed, and orientation realignment solves the misalignment between the sensor and body segment. Furthermore, the manually adjusted step detection was based on the IMU input and used in the KF for estimating the foot and CoM positions part. Here, based on the use of segment orientations and accelerations, the positions of both feet and CoM were derived. These positions, along with the relative distances and orientations, are used in the KF for estimating joint angles part to estimate and derive the joint angles. Finally, Post-processing calculates the joint positions and the segment orientations based on the positions and orientations of the feet and CoM, the joint angles and the relative distances.

2.6.1 KF for estimating foot and CoM positions

The orientations obtained from the IMUs were aligned with the segments, which provided the estimated orientations of the segments with respect to the world frame (${}^{W}\tilde{\boldsymbol{q}}_{B,Lf}$, ${}^{W}\tilde{\boldsymbol{q}}_{B,Rf}$, ${}^{W}\tilde{\boldsymbol{q}}_{B,Pel}$). Based on the method proposed by Refai et al. [15], using the gravity-free IMU accelerations (${}^{W}\tilde{\boldsymbol{a}}_{B,Lf}$, ${}^{W}\tilde{\boldsymbol{a}}_{B,Rf}$, ${}^{W}\tilde{\boldsymbol{a}}_{B,Pel}$) and the IMU orientations, the positions of the left foot, right foot, and the CoM (${}^{W}\tilde{\boldsymbol{p}}_{B,Lf}$, ${}^{W}\tilde{\boldsymbol{p}}_{B,Rf}$, ${}^{W}\tilde{\boldsymbol{p}}_{B,CoM}$) were estimated. In [15], it is assumed that the accelerations at the CoM are similar to the accelerations measured by the IMU located at the pelvis (${}^{W}\tilde{\boldsymbol{a}}_{B,Pel}$). This method [15] assumes that the moment about the CoM is zero and that the CMP overlaps with the Zero Moment Point (ZMP), which can also be defined as the Centre of Pressure for flat ground surfaces [20]. This allows the movement of the CoM to be linked to the stance foot, thus restricting drift between the feet and the CoM.

2.6.2 KF for estimating joint angles

In this section, the joint angles of the lower body ($\tilde{\Theta}L$ and $\tilde{\Theta}R$) are estimated using the estimated foot and CoM positions (${}^{W}\tilde{\boldsymbol{p}}_{B,Lf}$, ${}^{W}\tilde{\boldsymbol{p}}_{B,Rf}$, ${}^{W}\tilde{\boldsymbol{p}}_{B,Pel}$) and biomechanical constraints within a forward kinematic chain-based constrained Kalman filter (FKC-CMP). This was achieved using a smooth prediction model, illustrated here with the left leg as an example:

$$\tilde{\mathbf{\Theta}}_{L,k} = \tilde{\mathbf{\Theta}}_{L,k-1} + \boldsymbol{w}_k \tag{4}$$

where $\boldsymbol{w}_k$ represents the process noise vector. This process noise is controlled by the covariance matrix $\boldsymbol{Q}$. The biomechanical constraints consist of three parts:
1) The joint range of motions (ROM), stated in (5), which are based on the model of Arnold et al. [21], which is used by OpenSim software.

$$\begin{aligned} \mathbf{\Theta}_{min} \leq \mathbf{\Theta}_L \leq \mathbf{\Theta}_{max} \\ \mathbf{\Theta}_{min} \leq \mathbf{\Theta}_R \leq \mathbf{\Theta}_{max} \end{aligned} \tag{5}$$

The other two biomechanical constraints are established in the following text. The estimated left foot position and orientation of the IMU with respect to the CoM, expressed in the pelvis frame were calculated as:

$${}^{B,Pel}\tilde{\boldsymbol{p}}_{B,Lf} = {}^{W}\tilde{\boldsymbol{q}}_{B,Pel}{}^{-1} \times ({}^{W}\tilde{\boldsymbol{p}}_{B,Lf} - {}^{W}\tilde{\boldsymbol{p}}_{CoM}) \tag{6}$$

$${}^{B,Pel}\tilde{\boldsymbol{q}}_{B,Lf} = {}^{W}\tilde{\boldsymbol{q}}_{B,Pel}{}^{-1} \otimes {}^{W}\tilde{\boldsymbol{q}}_{B,Lf} \tag{7}$$

According to the forward kinematics of the lower body model as shown in Figure 1, the IMU left foot position was defined as:

$$\begin{bmatrix} {}^{B,Pel}\hat{\boldsymbol{p}}_{IMU,Lf} \\ 0 \end{bmatrix} = {}^{B,Pel}\hat{\boldsymbol{T}}_{B,Lt}(\theta_{Lh,Y}, \theta_{Lh,X}, \theta_{Lh,Y})\, {}^{B,Lt}\hat{\boldsymbol{T}}_{B,Ls}(\theta_{Lk,Y})\, {}^{B,Ls}\hat{\boldsymbol{T}}_{B,Lf}(\theta_{La,Y}) \begin{bmatrix} {}^{B,Lf}\bar{\boldsymbol{d}}_{IMU/La} \\ 0 \end{bmatrix} \tag{8}$$

where ${}^{B,Pel}\hat{\boldsymbol{T}}_{IMU,Lt}$, ${}^{B,Lt}\hat{\boldsymbol{T}}_{IMU,Ls}$, and ${}^{B,Ls}\hat{\boldsymbol{T}}_{IMU,Lf}$ were the transformation matrices between two joints. These transformation matrices were defined as:

$${}^{B,Pel}\hat{\boldsymbol{T}}_{IMU,Lt} = \begin{bmatrix} {}^{B,Pel}\hat{\boldsymbol{R}}_{B,Lt} & {}^{B,Pel}\bar{\boldsymbol{d}}_{Lh/CoM} \\ 0 & 0 \end{bmatrix} \tag{9}$$

$${}^{B,Lt}\hat{\boldsymbol{T}}_{IMU,Ls} = \begin{bmatrix} {}^{B,Lt}\hat{\boldsymbol{R}}_{B,Ls} & {}^{B,Lt}\bar{\boldsymbol{d}}_{Ls/Lt} \\ 0 & 0 \end{bmatrix} \tag{10}$$

$${}^{B,Ls}\hat{\boldsymbol{T}}_{IMU,Lf} = \begin{bmatrix} {}^{B,Ls}\hat{\boldsymbol{R}}_{B,Lf} & {}^{B,Ls}\bar{\boldsymbol{d}}_{Lf/Ls} \\ 0 & 0 \end{bmatrix} \tag{11}$$

where ${}^{B,Pel}\hat{\boldsymbol{R}}_{B,Lt}$, ${}^{B,Lt}\hat{\boldsymbol{R}}_{B,Ls}$, and ${}^{B,Ls}\hat{\boldsymbol{R}}_{B,Lf}$ were derived from ${}^{B,Pel}\hat{\boldsymbol{q}}_{B,Lt}$, ${}^{B,Lt}\hat{\boldsymbol{q}}_{B,Ls}$, and ${}^{B,Ls}\hat{\boldsymbol{q}}_{B,Lf}$ by using the quaternion to rotation matrix algorithm. The forward left foot orientation was defined as:

$${}^{B,Pel}\hat{\boldsymbol{q}}_{B,Lf} = {}^{B,Pel}\hat{\boldsymbol{q}}_{B,Lt}(\theta_{Lh,Y}, \theta_{Lh,X}, \theta_{Lh,Z}) \otimes {}^{B,Lt}\hat{\boldsymbol{q}}_{B,Ls}(\theta_{Lk,Y}) \otimes {}^{B,Ls}\hat{\boldsymbol{q}}_{B,Lf}(\theta_{La,Y}) \tag{12}$$

where ${}^{B,Pel}\hat{\boldsymbol{q}}_{B,Lt}$, ${}^{B,Lt}\hat{\boldsymbol{q}}_{B,Ls}$, and ${}^{B,Ls}\hat{\boldsymbol{q}}_{B,Lf}$ were the rotations between two connected segment frames, which follow the Y-X-Z sequence.

Based on (6)-(12), the other two constraints are:
2) The equality between the estimated foot position based on the IMU data and the forward kinematic estimated position of the foot, both with respect to the CoM in the pelvis frame. This can be written as:

$${}^{B,Pel}\hat{\boldsymbol{p}}_{IMU,Lf}(\tilde{\mathbf{\Theta}}_L) = {}^{B,Pel}\tilde{\boldsymbol{p}}_{IMU,Lf} \tag{13}$$

3) The equality between the estimated and forward foot orientations, both with respect to the pelvis frame. This can be written as:

$${}^{B,Pel}\hat{\boldsymbol{q}}_{B,Lf}(\tilde{\mathbf{\Theta}}_L) = {}^{B,Pel}\tilde{\boldsymbol{q}}_{B,Lf} \tag{14}$$

Linearisation was done to both equality constraints using Taylor series approximation [22], enabling the use of these constraints in our linear KF estimator. This gives:

$$(\boldsymbol{D}_{pos})_{3\times5}(\tilde{\mathbf{\Theta}}_L)_{5\times1} = (\boldsymbol{d}_{pos})_{3\times1} + \boldsymbol{v}_{pos} \tag{15}$$

$$(\boldsymbol{D}_{ori})_{4\times5}(\tilde{\mathbf{\Theta}}_L)_{5\times1} = (\boldsymbol{d}_{ori})_{4\times1} + \boldsymbol{v}_{ori} \tag{16}$$

where the variables $\boldsymbol{D}_{pos}$ $\boldsymbol{D}_{ori}$, $\boldsymbol{d}_{pos}$, and $\boldsymbol{d}_{ori}$ can be found in Appendix A.
Obtaining the estimated foot positions and orientations from the IMUs introduced estimation errors. These

estimation errors are represented by $\boldsymbol{v}_{pos}$ and $\boldsymbol{v}_{ori}$. By adjusting the covariance matrices $\boldsymbol{R}_{pos}$ and $\boldsymbol{R}_{ori}$, the dependency of the joint angle estimates on the constraints can be changed. Based on [23], the constrained joint angles $\tilde{\boldsymbol{\Theta}}^{+}_{L,k}$ were estimated using a KF with state equality constraints.

To satisfy the inequality constraint (5), the following method was used:

$$\tilde{\boldsymbol{\Theta}}^{+}_{L,k} = \min(\boldsymbol{\Theta}_{max}, \max(\boldsymbol{\Theta}_{min}, \tilde{\boldsymbol{\Theta}}^{+}_{L,k})) \tag{17}$$

where, $\boldsymbol{\Theta}_{max}$ and $\boldsymbol{\Theta}_{min}$ are the maximum and minimum value respectively for the joint angle.

2.6.3 Post-processing

In the post-processing part, the the joint positions (RP) and the segment orientations (SO) are calculated based on the feet and CoM positions, the orientations of the feet and the pelvis, the joint angles, the relative distances (D), and relative distances between the foot IMU and locations around the foot (I). In section 2.6.1 were the estimated foot and CoM positions (${}^{W}\tilde{\boldsymbol{p}}_{B,Lf}$, ${}^{W}\tilde{\boldsymbol{p}}_{B,Rf}$, ${}^{W}\tilde{\boldsymbol{p}}_{B,CoM}$) and the associated orientations (${}^{W}\tilde{\boldsymbol{q}}_{B,Lf}$, ${}^{W}\tilde{\boldsymbol{q}}_{B,Rf}$, ${}^{W}\tilde{\boldsymbol{q}}_{B,Pel}$) already obtained. Based on these positions and orientations, the joint positions of the hip and the knee for both legs (${}^{W}\tilde{\boldsymbol{p}}_{Lh}$, ${}^{W}\tilde{\boldsymbol{p}}_{Lk}$, ${}^{W}\tilde{\boldsymbol{p}}_{Rh}$, ${}^{W}\tilde{\boldsymbol{p}}_{Rk}$) were calculated similarly using forward kinematics to (8). In a same fashion, the orientations of the thighs and the shanks of both legs (${}^{W}\tilde{\boldsymbol{q}}_{Lt}$, ${}^{W}\tilde{\boldsymbol{q}}_{Ls}$, ${}^{W}\tilde{\boldsymbol{q}}_{Rt}$, ${}^{W}\tilde{\boldsymbol{q}}_{Rs}$) were calculated using forward kinematics in a similar way to 12. Finally, based on assuming that the foot is a rigid body, the phalanges (toe) and ankle positions (${}^{W}\tilde{\boldsymbol{p}}_{Lp}$, ${}^{W}\tilde{\boldsymbol{p}}_{La}$, ${}^{W}\tilde{\boldsymbol{p}}_{Rp}$, ${}^{W}\tilde{\boldsymbol{p}}_{Ra}$) were calculated using a translation of the foot position. The method used to calculate these positions for the left leg is defined as:

$${}^{W}\tilde{\boldsymbol{p}}_{Lp} = {}^{W}\tilde{\boldsymbol{p}}_{B,Lf} - {}^{W}\tilde{\boldsymbol{q}}_{B,Lf} \times {}^{B,Lf}\bar{\boldsymbol{d}}_{IMU/Lp} \tag{18}$$

$${}^{W}\tilde{\boldsymbol{p}}_{La} = {}^{W}\tilde{\boldsymbol{p}}_{B,Lf} - {}^{W}\tilde{\boldsymbol{q}}_{B,Rf} \times {}^{B,Lf}\bar{\boldsymbol{d}}_{IMU/La} \tag{19}$$

2.7 Estimator parameters

The initial positions and velocities of the feet and the CoM are derived from Vicon data. Additionally, the initial joint angles are also obtained from Vicon data. Also, the step detection manually corrected by Luke Sy was used as input. The Joint angles part used covariance matrix $\boldsymbol{P}_0$, which was set to $0.0001\boldsymbol{I}_{5\times5}$. Furthermore, the covariance parameters were set to $\boldsymbol{Q} = 0.03^2\boldsymbol{I}_{5\times5}$, $\boldsymbol{R}_{pos} = 0.001^2\boldsymbol{I}_{3\times3}$, and $\boldsymbol{R}_{ori} = 0.05^2\boldsymbol{I}_{9\times9}$.

2.8 Evaluation metrics

2.8.1 Relative position RMSEs

To assess the accuracy of the estimated relative positions, we compared the relative foot position RMSEs obtained from two different methods with those reported by Sy et al. [11].
Firstly, based on the positions output from the KF for estimating foot and CoM positions, the CoM position was subtracted from each foot position to obtain the relative position between CoM and foot. Then, by comparing the relative positions obtained from our method with the VICON relative positions, we calculated the RMSEs of the relative foot positions. Finally, we calculated the relative position RMSEs using the relative foot positions reported by Sy et al., and compared them to our results.

2.8.2 Joint angle RMSEs for different inputs

In order to validate the effectiveness of the estimated joint angles of the proposed method, we compared the RMSEs between the estimated joint angles with different inputs and the Vicon reference.
Firstly, we used the Vicon reference position and orientation of the feet and the pelvis as the input of the KF for estimating joint angles, which was aimed to verify whether the method can accurately estimate joint angles if accurate feet and pelvis positions and orientations are provided. Secondly, we replaced either the reference position or orientations with estimated ones to verify how position and orientation estimations influence the joint angles estimation results. We also compared our results with Sy et al. [11].

2.8.3 Joint position and segment orientation RMSEs

To evaluate the estimated joint positions and segment orientations, we compared the joint position RMSEs and segment orientation RMSEs with those reported in other literature.

Mean position e_{pos} and orientation e_{ori} RMSEs are metrics commonly used in other IMCs [24], [11]. To prevent drift due to the lack of an external global position reference, the CoM position was set as the origin. This was used for both measured and reference data (i.e., the reference origin is set to the reference CoM position). These positions were for each hip, knee, phalanges and ankle, given by: $RP = \{R_h, R_k, R_p, R_a, L_h, L_k, L_p, L_a\}$ and e_{pos} was calculated as:

$$e_{pos} = \frac{1}{N_k N_{pos}} \sum_{k=1}^{N_k} \sum_{i \in RP} ||^W \boldsymbol{p}_{i,k}^{ref} -^W \tilde{\boldsymbol{p}}_{i,k}||^2 \tag{20}$$

where the number of joints $N_{pos} = 8$, ${}^W\boldsymbol{p}_{i,k}^{ref}$ are the joint positions based on the Vicon data, and N_k is the number of total samples of each trial.

The RMSE orientation error was calculated using the sum of squared L2-norm [24], [11]. With all segment orientations given by $SO = \{Pel, Rt, Rs, Rf, Lt, Ls, Lf\}$, e_{ori} was calculated as:

$$e_{ori} = \frac{1}{N_k N_{ori}} \sum_{k=1}^{N_k} \sum_{i \in SO} ||\log(^W \boldsymbol{q}_{B,i,k}^{ref} \otimes^W \tilde{\boldsymbol{q}}_{B,i,k}{}^{-1})^{\text{v}}||^2 \tag{21}$$

where the number of orientations $N_{ori} = 7$, ${}^W\boldsymbol{q}_{B,i,k}^{ref}$ is the segment orientation based on Vicon data, and the v-operator is used to extract the coordinates of the skew-symmetric matrix. Both e_{pos} and e_{ori} results will be compared to the findings of Sy et al. [11] [8].

2.8.4 Joint angle RMSEs and correlation coefficients (CCs)

In order to evaluate the joint angles estimated by the proposed method, we compared the joint angle RMSEs and CCs across all trials to those reported in other literature.

Both RMSE and CC of each angle of Θ_R and Θ_L were calculated for each trial and also given by mean and SD for every task. These joint angle RMSEs and CCs are commonly used in gait analysis papers, and we will compare our results with the work of Sy et al. [11] [8].

2.8.5 Straight Walk RMSEs

To evaluate the joint angles during straight-line walking, we compared the RMSEs of the hips, knees, and ankles for both legs.

During the walking trial, subjects turned 180 degrees and walked back. To eliminate any negative effects from this turn, the moment of turning was omitted from the dataset, resulting in an RMSE for straight-line walking. Then, the average angle of all hip angles (both legs) was calculated. Similarly, the average of knee and ankle angles of both legs was determined.

3 Results

3.1 Relative position RMSEs

Using the CMP update results in a relative position estimate that aligns with the reference, as shown in Figure 3.

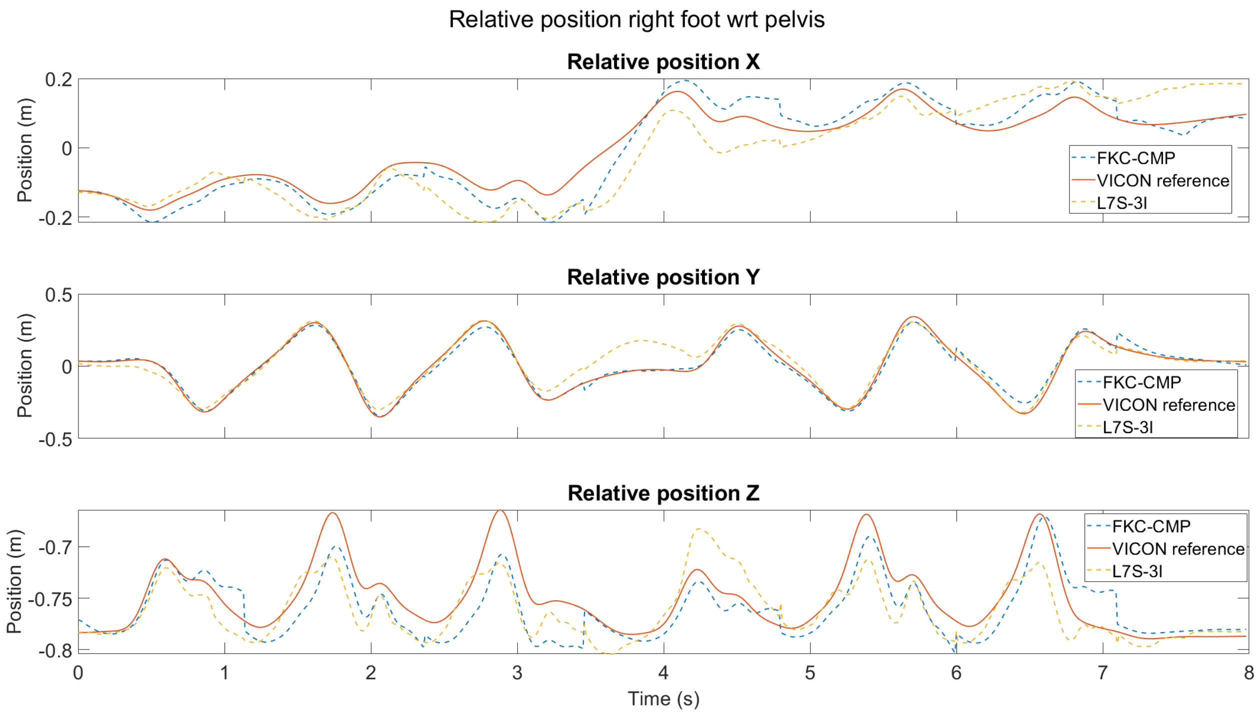

Figure 3: The relative distance RMSE of the walk trial between the right foot and the pelvis was estimated using the FKC-CMP algorithm (blue) and compared to L7S-3I (yellow) [11] and the VICON reference (red). This is an example of a walk trial.

The FKC-CMP is relatively successful in following the reference for the X-axis. For the Y-axis, our method can follow the reference, even during the turnaround $t = 4$ s, while the L7S-3I method has a large offset compared to the reference. The results for the Z-axis show a more similar outcome. In Figure 4, you can see that the relative RMSE for the Y-axis of FKC-CMP is smaller for both feet compared to L7S-3I. However, for the X-axis, the RMSE for the right foot is equal between the two, while for the left foot, the RMSE of L7S-3I is smaller. Additionally, the RMSEs for the Z-axis are nearly identical.

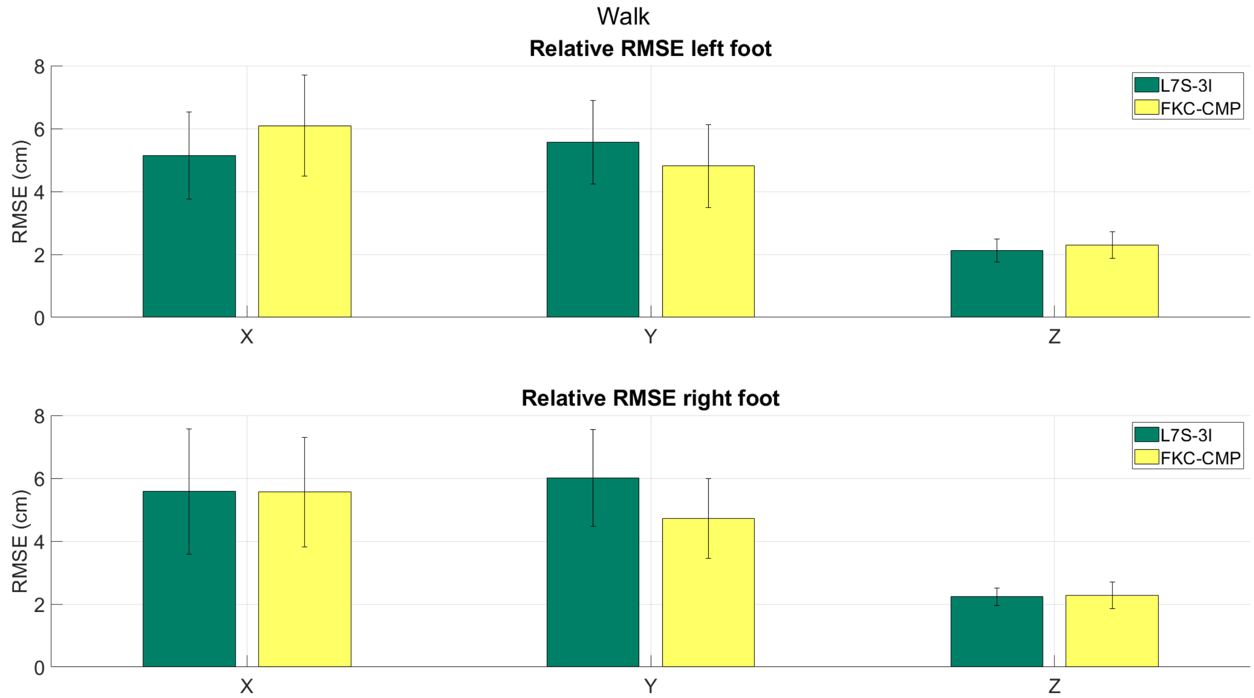

Figure 4: The relative distance RMSE of the walk trial is presented using two different algorithms. The estimates are provided for the left foot (top) and right foot (bottom). These RMSEs were calculated based on the positions by Sy et al. [11] (L7S-3I) and by the FKC-CMP algorithm.

3.2 Joint angle RMSEs for different inputs

3.2.1 Vicon reference input

Using the FKC-CMP algorithm with Vicon reference input results in accurate joint angle estimates with low RMSE values.
In Figure 5, the joint angle estimates are displayed for the FKC-CMP algorithm using three different sets of inputs, combined with the Vicon reference. Using Vicon input (yellow) results in the best estimates for the joint angles.

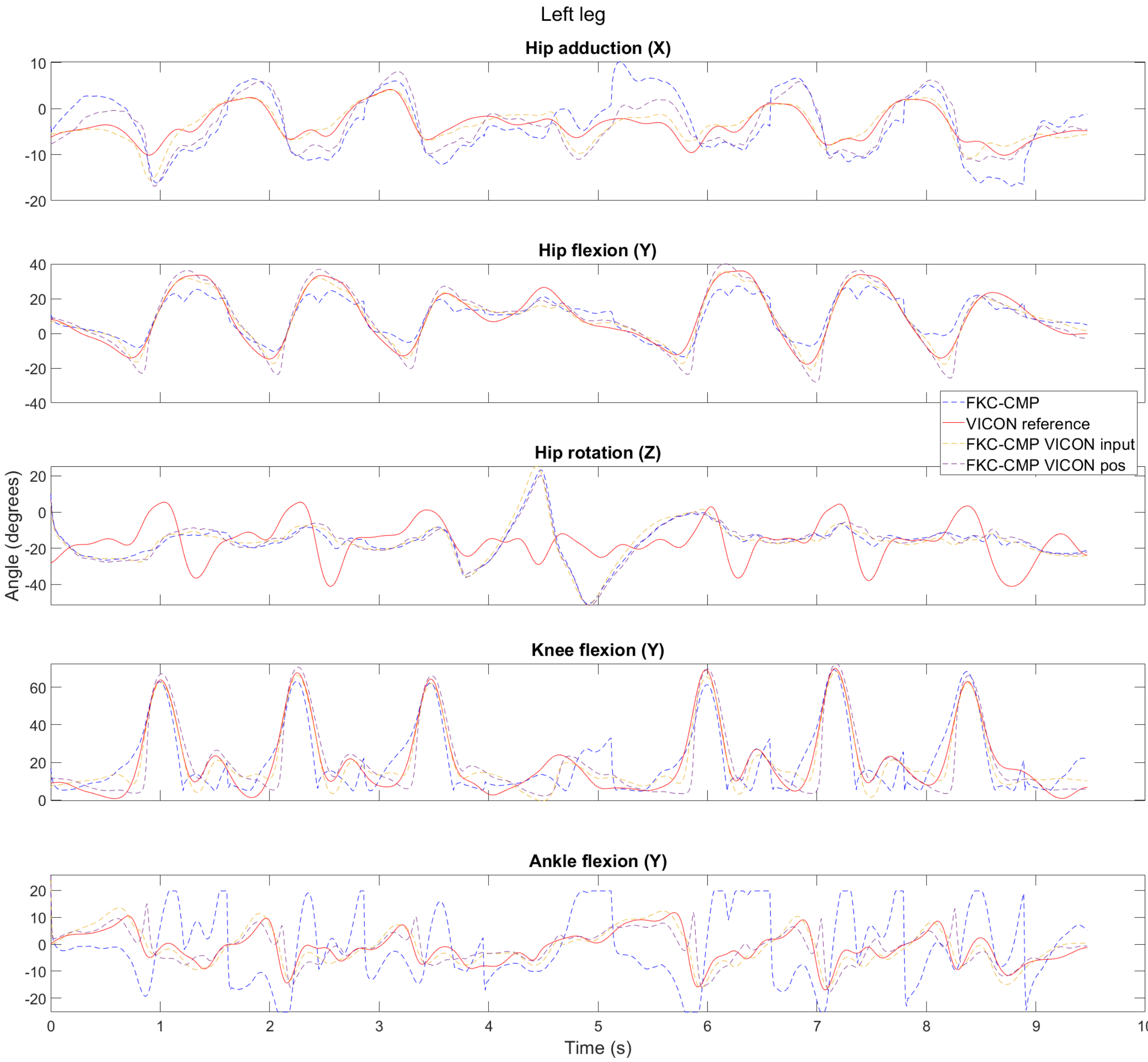

Figure 5: The joint angle estimates of a walk trial for the hip (X, Y, and Z), knee (Y), and ankle (Y) were evaluated using three different inputs. For FKC-CMP (blue), estimated positions and orientations were used. For FKC-CMP VICON input (yellow), Vicon positions and orientations were used. For FKC-CMP VICON pos (purple), Vicon positions combined with estimated orientations were used. These three sets of estimates are plotted against the VICON reference (red).

Furthermore, in Figure 6, the RMSE values for each angle are given for the FKC-CMP algorithm using different inputs. The RMSE values for each angle, when using Vicon position and orientation input (FKC-CMP VICON input), indicate that using the reference as input results in accurate joint angles with low RMSE values. An exception is the hip Z angle, which shows RMSE values of 10.9° and 15.3° for the right and left leg, respectively.

3.2.2 Impact of different input

Using the estimated orientation provided by the IMUs results in larger RMSE values.
In Figure 6, when using the estimated orientation provided by the IMUs along with the Vicon position (FKC-CMP VICON pos), the RMSE values for each angle are larger compared to the RMSEs obtained with the fully Vicon reference input (FKC-CMP VICON input). Comparing the RMSEs provided by the algorithm using both estimated position and orientation (FKC-CMP) to the RMSEs obtained using Vicon position and estimated orientation (FKC-CMP VICON pos) reveals only minor differences in RMSE for most angles. However, an exception is the ankle angle, where the RMSE increases from around 5° up to 15°.

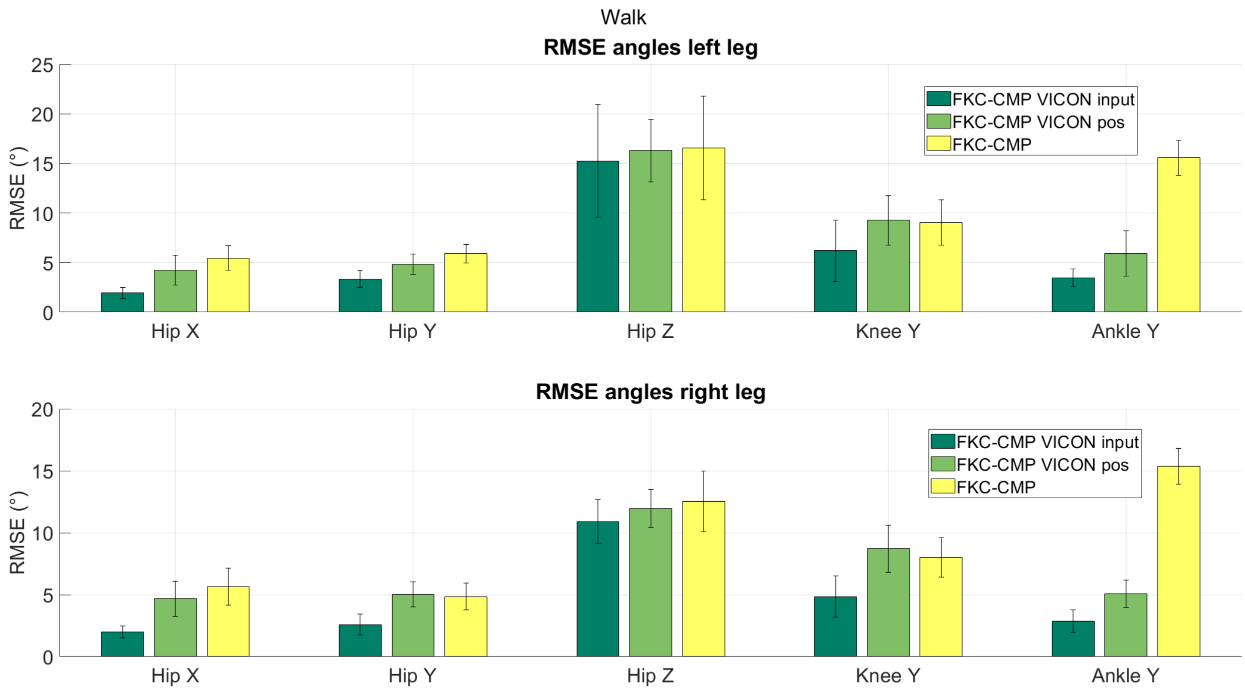

Figure 6: The joint angles of the hip (X, Y and Z), knee (Y) and ankle (Y) were estimated for different inputs of the algorithm. The first column displays the RMSEs of the algorithm using Vicon reference position and orientation input (FKC-CMP VICON input). The next column shows the RMSEs of the algorithm with Vicon position and estimated orientation (FKC-CMP no PM). Finally, the RMSEs of the algorithm using estimated position and estimated orientation (FKC-CMP) as input are presented.

3.3 Joint position and segment orientation RMSEs

The mean joint position RMSE and segment orientation RMSE of the FKC-CMP across all tasks and subjects were 6.2 ± 3.6 cm was 11.5 ± 5.9 °, respectively.
In Table 1, the joint position RMSE for FKC-CMP, averaged across all tasks and subjects, is slightly higher but comparable to CKF-3IMU and L7S-3I. However, the standard deviation of 3.6, compared to the other standard deviations of 1.3, suggests a higher variance in our estimated joint positions. The segment orientation RMSE, averaged across all tasks and subjects, is lower than those reported in related literature. However, the standard deviation of the segment orientation RMSE for L7S-3I is significantly lower than the other two RMSEs.

Table 1: Mean joint position and segment orientation RMSEs of the proposed FKC-CMP, across all tasks and all subjects and related literature.

	FKC-CMP	CKF-3IMU [8]	L7S-3I [11]
e_{pos} (cm)	6.2 (3.6)	5.2 (1.3)	5.9 (1.3)
e_{ori} (°)	11.5 (5.9)	18.9 (5.3)	13.4 (1.9)

3.4 Joint angle RMSEs and correlation coefficients (CCs)

The hip Z angle and the ankle Y angle both have high joint angle RMSE values and low CC values, indicating poor joint angle estimation. In contrast, the hip X, Y, and knee Y angles show more promising RMSE and CC values, indicating more acceptable joint angle estimations.
In Figure 7, the RMSE values for the left leg are slightly higher compared to those for the right leg. Specifically, the hip Z-angle of the left leg is significantly higher than the same angle of the right leg. Additionally, looking at the CC values, the hip Z angles for the left leg are around zero, while the hip Z-axis angles for the right leg perform better with values around 0.4. Finally, both ankle angles have higher RMSE values compared to other angles, and their CC values are close to zero.

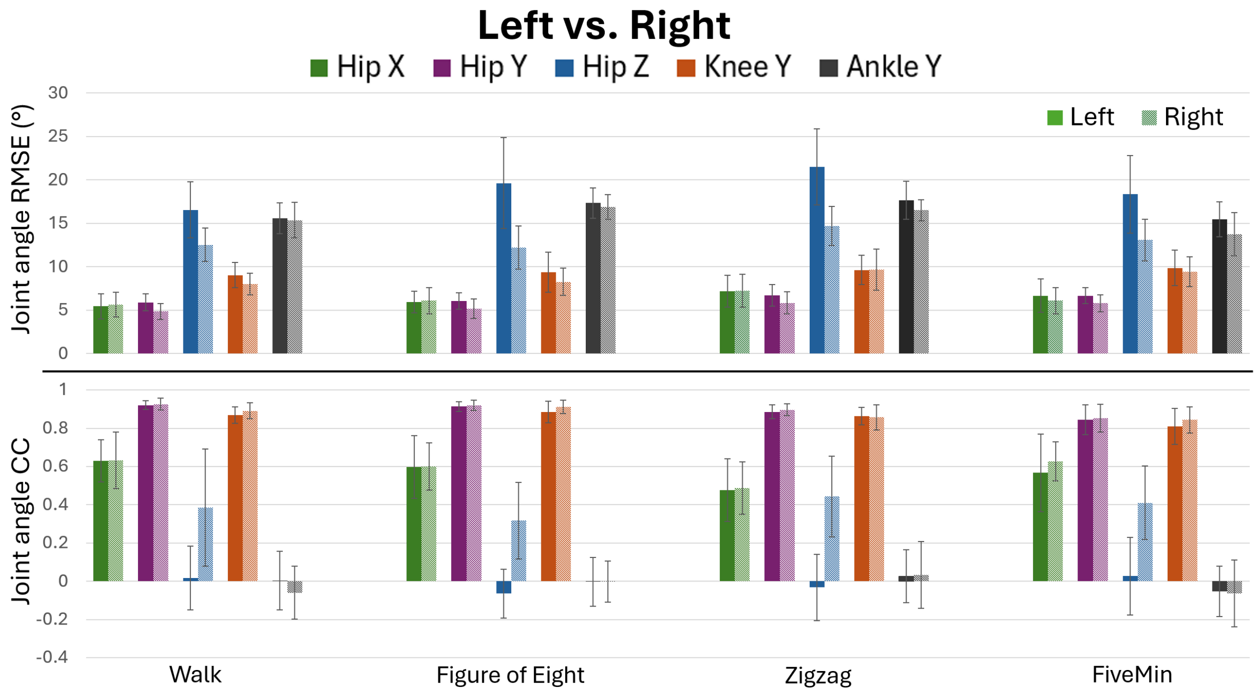

Figure 7: The joint angle RMSE and CC are shown for each angle across all tasks. The different colours indicate different angles. The full coloured columns belong to the left leg and the gradient columns to the right leg.

3.5 Straight Walk RMSEs

Comparing our FKC-CMP algorithm to other literature shows comparable values for the knee, while the hip RMSE is larger than both other works. However, in Table 2, the ankle shows a significantly larger RMSE value compared to L7S-3I.

Table 2: Mean joint angle RMSEs of the proposed FKC-CMP, during straight walking across all subjects and related literature.

Algorithm	FKC-CMP	CKF-3IMU [8]	L7S-3I [11]
Hip RMSE (°)	6.7 (3.8)	4.4 (1.9)	5.0 (1.0)
Knee RMSE (°)	7.7 (1.7)	5.7 (2.2)	8.2 (2.2)
Ankle RMSE (°)	15.0 (2.0)	-	5.9 (1.6)

4 Discussion

4.1 Relative position RMSEs

Compared to Sy et al. [11], our CMP update seems to perform better than the pseudo-measurement (PM) method in reducing drift of the relative position between pelvis and foot. While the relative RMSEs are similar for the Z-axis and similar or worse for the X-axis, the relative RMSEs are better for the Y-axis. This suggests that the CMP update outperforms the pelvis PM used by Sy et al. [11].
Furthermore, the positions in our work are estimated after the KF for estimating the feet and CoM positions part and do not incorporate constraints. In contrast, Sy et al. use constraints such as fixed leg lengths and a hinged knee joint to determine the feet and CoM positions. Despite using fewer constraints and thus less information, this emphasizes that the CMP update seems to perform better than the PM used by Sy et al. [11].

4.2 Joint angle RMSEs for different inputs

In Figure 5, the Vicon reference for the left hip rotation angle indicates rotations occurring during the walk, ranging from 0 degrees to -40 degrees. However, when inspecting the data, this rotation is observed only for the left leg and not for the right leg. Additionally, in Figure 7, the CC values for the left leg hip rotation are almost zero, while the CC values for the right leg hip rotation are around 0.4, indicating a weak but present correlation between the Vicon reference and the estimated hip rotation. Moreover, when inspecting the walk trial data, there is no movement which requires such a hip rotation. This suggests that the Vicon reference hip rotation data may be inaccurate. This could potentially be due to poor calibration, marker placement, or because the Vicon system has difficulty with detecting hip rotations due to the subtle nature of these movements.
Furthermore, the ankle flexion estimates for FKC-CMP are highly volatile, often reaching the maximum and minimum angles of 20 and -25 degrees. However, when comparing the FKC-CMP estimates to the FKC-CMP VICON input estimates, it is clear that the algorithm can provide accurate ankle estimates when given correct positions and orientations. This indicates that inaccuracies in positions, orientations, or other joint angle estimates significantly impair the algorithm's ability to measure accurate ankle flexion.
Finally, the algorithm appears to handle singularities effectively. For instance, when the knee is extended, the relative distance between the hip and the ankle for each foot increases as expected, but does not take disproportionally large values.

4.3 Comparing RMSE values to other literature

Comparing our joint position RMSE and segment orientation RMSE to other literature in Table 1, shows overall comparable results. However, the notably higher standard deviation for joint position RMSE suggests a high variance in estimating the joint positions. This could be attributed to the calculation of the ankle and phalanges positions, which are derived from the foot position. Therefore, any inaccuracies in the foot position estimate will proportionally affect the estimates for the ankle and phalanges positions.
The FKC-CMP algorithm in Figure 7 shows that both RMSE values and CC values are consistent among the different walking tasks. Additionally, the RMSE and CC values are comparable between the left and right leg, except for the hip Z angle.
Comparing the straight walk RMSEs to other literature in Table 2 shows that our algorithm performs similarly for the hip and the knee angles, while performing significantly worse for the ankle angle. This large ankle angle RMSE was already present in other tasks and still occurs during a straight walking task. Therefore, comparing the performance of our algorithm to those in other literature suggests that our algorithm is better suited for walking tasks involving varied movements, while other algorithms may be more appropriate for straight-line walking tasks.

4.4 Limitations

One limitation of the FKC-CMP algorithm is the need for initial values. If there is no Vicon available providing these initial values, they can be obtained through other means. For example, segment lengths can be measured using a tape measure. These measurements are crucial for forward kinematics and must be accurate. Furthermore, initial angles can be estimated by assuming a pose that sets all joint angles to known values for that specific position.
Another limitation is that the algorithm in this research uses step data, which was provided by Sy et al. [8]

in their dataset. Therefore, when using other data, a step detection algorithm is necessary to accurately identify when a step occurs.

4.5 Future work

Currently, our algorithm first uses a KF to estimate the positions of the feet and the CoM, and then uses this information in another KF to estimate the joint angles using constraints. These two processes could be combined, which could enhance the accuracy of position estimates by applying the constraints from the second KF to the initial position estimation. More accurate position estimates could subsequently improve the joint angle estimates and overall lower-body kinematics.

Furthermore, for future use, the accuracy of ankle joint estimates needs improvement. Currently, the results indicate that the algorithm cannot accurately estimate the ankle joint with the current position and orientation estimates. While Figure 6 shows that accurate position and orientation data can lead to precise ankle joint angle estimates, achieving such accuracy in real-world measurements is challenging. Therefore, another method that provides accurate ankle angle measurements is necessary to enhance the FKC-CMP algorithm.

5 Conclusion

This paper presents a forward kinematics chain-based constrained Kalman filter to estimate lower-body kinematics during walking using a small set of IMUs. Using walking tasks data from an online dataset, the mean joint position RMSE and segment orientation RMSE across all tasks and subjects were 6.2 ± 3.6 cm and $11.5 \pm 5.9°$, respectively, indicating a reasonable level of accuracy.

Furthermore, the algorithm was able to estimate most joint angles well, but requires improvement for the ankle joint estimation.

Future work should focus on refining the ankle joint estimates, as the current method lacks precision. Additionally, combining the two Kalman filters could enhance the accuracy of position estimates, subsequently improving the joint angle estimates and overall lower-body kinematics.

References

[1] Chien Ke Liao, Chung Dial Lim, Ching Ying Cheng, Cheng Ming Huang, and Li Chen Fu. Vision based gait analysis on robotic walking stabilization system for patients with parkinson's disease. *IEEE International Conference on Automation Science and Engineering*, 2014-January:818–823, 2014.

[2] Rania Kolaghassi, Mohamad Kenan Al-Hares, and Konstantinos Sirlantzis. Systematic review of intelligent algorithms in gait analysis and prediction for lower limb robotic systems. *IEEE Access*, 9:113788–113812, 2021.

[3] Diego Guffanti, Alberto Brunete, and Miguel Hernando. Development and validation of a ros-based mobile robotic platform for human gait analysis applications. *Robotics and Autonomous Systems*, 145:103869, 11 2021.

[4] Antoine Muller, Hakim Mecheri, Philippe Corbeil, André Plamondon, and Xavier Robert-Lachaine. Inertial motion capture-based estimation of l5/s1 moments during manual materials handling. *Sensors*, 22:6454, 9 2022.

[5] Eline M. Nijmeijer, Pieter Heuvelmans, Ruben Bolt, Alli Gokeler, Egbert Otten, and Anne Benjaminse. Concurrent validation of the xsens imu system of lower-body kinematics in jump-landing and change-of-direction tasks. *Journal of Biomechanics*, 154, 6 2023.

[6] Eduardo Palermo, Stefano Rossi, Francesca Marini, Fabrizio Patanè, and Paolo Cappa. Experimental evaluation of accuracy and repeatability of a novel body-to-sensor calibration procedure for inertial sensor-based gait analysis. *Measurement*, 52:145–155, 6 2014.

[7] Alberto Leardini, Alberto Chiari, Ugo Della Croce, and Aurelio Cappozzo. Human movement analysis using stereophotogrammetry: Part 3. soft tissue artifact assessment and compensation. *Gait & Posture*, 21:212–225, 2 2005.

[8] Luke Sy, Michael Raitor, Michael Del Rosario, Heba Khamis, Lauren Kark, Nigel H. Lovell, and Stephen J. Redmond. Estimating lower limb kinematics using a reduced wearable sensor count. *IEEE Transactions on Biomedical Engineering*, 68:1293–1304, 4 2021.

[9] Shigeru Tadano, Ryo Takeda, and Hiroaki Miyagawa. Three dimensional gait analysis using wearable acceleration and gyro sensors based on quaternion calculations. *Sensors 2013, Vol. 13, Pages 9321-9343*, 13:9321–9343, 7 2013.

[10] Manon Kok, Jeroen D. Hol, and Thomas B. Schön. Using inertial sensors for position and orientation estimation. *Foundations and Trends in Signal Processing*, 11:1–153, 2017.

[11] Luke Wicent Sy, Nigel H. Lovell, and Stephen J. Redmond. Estimating lower body kinematics using a lie group constrained extended kalman filter and reduced imu count. *IEEE Sensors Journal*, 21:20969–20979, 9 2021.

[12] Salvatore Tedesco, John Barton, and Brendan O'Flynn. A review of activity trackers for senior citizens: Research perspectives, commercial landscape and the role of the insurance industry. *Sensors (Basel, Switzerland)*, 17, 6 2017.

[13] D. Roetenberg, H. Luinge, and P. Slycke. Xsens mvn: Full 6dof human motion tracking using miniature inertial sensors. 2009.

[14] Mohamed Irfan Mohamed Refai, Bert Jan F. Van Beijnum, Jaap H. Buurke, Mique Saes, Johannes B.J. Bussmann, Carel G. Meskers, Erwin Van Wegen, Gert Kwakkel, and Peter H. Veltink. Portable gait lab: Zero moment point for minimal sensing of gait. *Annual International Conference of the IEEE Engineering in Medicine and Biology Society. IEEE Engineering in Medicine and Biology Society. Annual International Conference*, 2019:2077–2081, 7 2019.

[15] Mohamed Irfan Mohamed Refai, Bert Jan F. Van Beijnum, Jaap H. Buurke, and Peter H. Veltink. Portable gait lab: Tracking relative distances of feet and com using three imus. *IEEE Transactions on Neural Systems and Rehabilitation Engineering*, 28:2255–2264, 10 2020.

[16] Isaac Skog, John Olof Nilsson, Dave Zachariah, and Peter Handel. Fusing the information from two navigation systems using an upper bound on their maximum spatial separation. *2012 International Conference on Indoor Positioning and Indoor Navigation, IPIN 2012 - Conference Proceedings*, 2012.

[17] Hongyu Zhao, Zhelong Wang, Sen Qiu, Yanming Shen, Luyao Zhang, Kai Tang, and Giancarlo Fortino. Heading drift reduction for foot-mounted inertial navigation system via multi-sensor fusion and dual-gait analysis. *IEEE Sensors Journal*, 19:8514–8521, 10 2019.

[18] Mtw awinda user manual — movella.com.

[19] Sebastian O. H. Madgwick. An efficient orientation filter for inertial and inertial / magnetic sensor arrays. 2010.

[20] Marko B. Popovic, Ambarish Goswami, and Hugh Herr. Ground reference points in legged locomotion: Definitions, biological trajectories and control implications. *http://dx.doi.org/10.1177/0278364905058363*, 24:1013–1032, 12 2005.

[21] Edith M. Arnold, Samuel R. Ward, Richard L. Lieber, and Scott L. Delp. A model of the lower limb for analysis of human movement. *Annals of Biomedical Engineering*, 38:269–279, 2 2010.

[22] M. T. Timpledon, S. F. Marseken, and L. M. Surhone. *Jacobian Matrix and Determinant: Vector Calculus, Partial Derivative, Vector Space, Euclidean Space, Gradient, Carl Gustav Jacob Jacobi, Tangent Space, Pushforward (differential), Directional Derivative*. Betascript Publishing, 2010.

[23] Dan Simon and Tien L.I. Chia. Kalman filtering with state equality constraints. *IEEE Transactions on Aerospace and Electronic Systems*, 38:128–136, 1 2002.

[24] T. von Marcard, B. Rosenhahn, M. J. Black, and G. Pons-Moll. Sparse inertial poser: Automatic 3d human pose estimation from sparse imus. *Eurographics Symposium on Geometry Processing*, 36:349–360, 3 2017.

A Linearisation of nonlinear equality constraints

Equation (14) can be simplified, written as:

$$f(\tilde{\boldsymbol{\Theta}}_L)_{4\times 1} = ({}^{B,Pel}\tilde{\boldsymbol{q}}_{B,Lf})_{4\times 1} \tag{22}$$

Firstly, the partial derivatives of $f(\tilde{\boldsymbol{\Theta}}_L)$ with respect to $(\tilde{\boldsymbol{\Theta}}_L)$ (also known as Jacobian matrix) is calculated using the partial derivatives method of a vector function with respect to a variable vector in matrix calculus [22], which gives:

$$\frac{\partial f\left(\tilde{\boldsymbol{\Theta}}_L\right)}{\partial \tilde{\boldsymbol{\Theta}}_L} = \begin{bmatrix} \left(\frac{\partial f(\tilde{\boldsymbol{\Theta}}_L)_{11}}{\partial \tilde{\boldsymbol{\Theta}}_L}\right)_{1\times 5} \\ \left(\frac{\partial f(\tilde{\boldsymbol{\Theta}}_L)_{21}}{\partial \tilde{\boldsymbol{\Theta}}_L}\right)_{1\times 5} \\ \left(\frac{\partial f(\tilde{\boldsymbol{\Theta}}_L)_{31}}{\partial \tilde{\boldsymbol{\Theta}}_L}\right)_{1\times 5} \\ \left(\frac{\partial f(\tilde{\boldsymbol{\Theta}}_L)_{41}}{\partial \tilde{\boldsymbol{\Theta}}_L}\right)_{1\times 5} \end{bmatrix}_{4\times 5} \tag{23}$$

Then via Taylor series approximation this can be linearised as in (24) and this provides the linearised constraint (16).

$$\underbrace{\left.\frac{\partial f\left(\tilde{\boldsymbol{\Theta}}_L\right)}{\partial \tilde{\boldsymbol{\Theta}}_L}\right|_{\tilde{\boldsymbol{\Theta}}_L=\tilde{\boldsymbol{\Theta}}^-_{L,k}}}_{(\boldsymbol{D}_{\text{ori}})_{4\times 5}} \tilde{\boldsymbol{\Theta}}_L = \underbrace{-f\left(\tilde{\boldsymbol{\Theta}}^-_{L,k}\right) + \left.\frac{\partial f\left(\tilde{\boldsymbol{\Theta}}_L\right)}{\partial \tilde{\boldsymbol{\Theta}}_L}\right|_{\tilde{\boldsymbol{\Theta}}_L=\tilde{\boldsymbol{\Theta}}^-_{L,k}} \tilde{\boldsymbol{\Theta}}^-_{L,k} + {}^{\text{B,Pel}}\tilde{\boldsymbol{q}}_{B,Lf}}_{(\boldsymbol{d}_{\text{ori}})_{4\times 1}} \tag{24}$$

Similarly, the same linearisation can be done for (13) to obtain (15).